

# 1,3,5-trinitro-1,3,5-triazine decomposition and chemisorption on Al(111) surface: First-principles molecular dynamics study

Naoto Umezawa,<sup>a)</sup> Rajiv K. Kalia, Aiichiro Nakano, and Priya Vashista

*Collaboratory for Advanced Computing and Simulations, University of Southern California, Los Angeles, California 90089-0242; Department of Chemical Engineering and Materials Science, University of Southern California, Los Angeles, California 90089-0242; Department of Computer Science, University of Southern California, Los Angeles, California 90089-0242; and Department of Physics and Astronomy, University of Southern California, Los Angeles, California 90089-0242*

Fuyuki Shimojo

*Department of Physics, Kumamoto University, Kumamoto 860-8555, Japan*

(Received 28 November 2005; accepted 4 April 2006; published online 15 June 2007)

We have investigated the decomposition and chemisorption of a 1,3,5-trinitro-1,3,5-triazine (RDX) molecule on Al(111) surface using molecular dynamics simulations, in which interatomic forces are computed quantum mechanically in the framework of the density functional theory (DFT). The real-space DFT calculations are based on higher-order finite difference and norm-conserving pseudopotential methods. Strong attractive forces between oxygen and aluminum atoms break N–O and N–N bonds in the RDX and, subsequently, the dissociated oxygen atoms and NO molecules oxidize the Al surface. In addition to these Al surface-assisted decompositions, ring cleavage of the RDX molecule is also observed. These reactions occur spontaneously without potential barriers and result in the attachment of the rest of the RDX molecule to the surface. This opens up the possibility of coating Al nanoparticles with RDX molecules to avoid the detrimental effect of oxidation in high energy density material applications. © 2007 American Institute of Physics.

[DOI: [10.1063/1.2200352](https://doi.org/10.1063/1.2200352)]

## I. INTRODUCTION

Aluminum powders are widely used as propellants, because their combustion products such as Al<sub>2</sub>O<sub>3</sub> are accompanied by a large amount of heat release.<sup>1</sup> In order to understand the combustion mechanisms and energetics,<sup>2,3</sup> there have been extensive studies of Al particles<sup>4,5</sup> and their oxidation.<sup>6–10</sup> Burn rates of propellants can be accelerated by reducing the size of Al particles, thereby increasing the surface to volume ratio and the rate of chemical reactions. A major technical difficulty for such small reactant particles is the dead weight of oxide layers. The thickness of the oxidized layer in an Al particle is known to be a few nanometers regardless of the particle size. Therefore, the ratio of the oxidized layer, which is not effective as a propellant, to the reactive portion increases for the smaller Al particles. This dead-weight problem in nanoscale reactant particles may be overcome by encapsulating the particles within complementary reactive materials,<sup>11–13</sup> such as nitramine hexahydro-1,3,5-trinitro-1,3,5-triazine (RDX, C<sub>3</sub>N<sub>6</sub>O<sub>6</sub>H<sub>6</sub>).<sup>14</sup>

Thermal decomposition of gas- and solid-phase RDX has been studied both experimentally and theoretically to understand the reaction pathways.<sup>15,16</sup> Although controversies exist among these studies, three plausible decomposition pathways have been identified: (1) ring fission of three CH<sub>2</sub>NNO<sub>2</sub> molecules, (2) N–N bond breaking resulting in

NO<sub>2</sub>, and (3) HONO elimination. Subsequent decompositions and the final products have also been studied in detail.

Although there are extensive experimental and theoretical studies of combustion of Al particle in air,<sup>17</sup> only a few<sup>18</sup> have reported its reaction characteristics with nitramine propellant such as RDX. In order to produce efficient high energy density Al/RDX nanocomposite materials, it is important to elucidate atomistic mechanisms of chemical reactions of RDX with Al.

We have performed first-principles molecular dynamics simulations to study the decomposition and chemisorption of a RDX molecule on Al(111) surface. Decomposition pathways of RDX and the oxidization of Al(111) surface are investigated in terms of Mulliken overlap populations and atomic charges. The simulation results show that RDX molecules are readily decomposed without potential barriers. This is in contrast to the decomposition of RDX in the absence of Al, where shock wave<sup>19</sup> or heat is required to overcome the potential barriers for decompositions. We will discuss the spontaneous reaction between RDX and Al(111) surface.

This paper is organized as follows. Simulation methods are presented in Sec. II and Sec. III contains simulation results. Finally, conclusions are given in Sec. IV.

## II. SIMULATION METHODS

In our first-principles molecular dynamics (MD) simulations, interatomic forces are calculated quantum mechanically in the framework of the density functional theory

<sup>a)</sup>Present address: National Institute for Materials Science, Ibaraki, 305-0044, Japan.

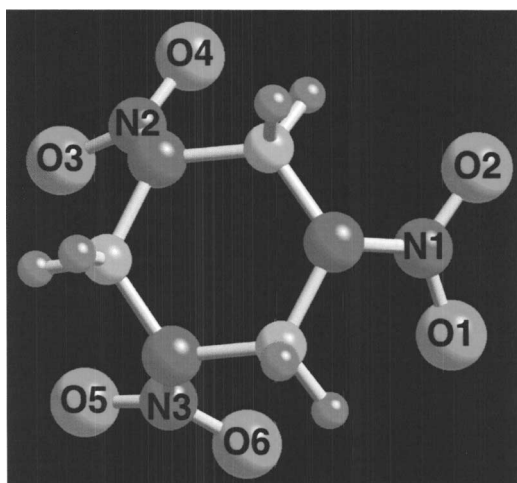


FIG. 1. A RDX molecule, where color represents atomic species: cyan for H, magenta for C, green for N, and red for O. The O atoms and the N atoms bonded to them are numbered for analysis.

(DFT),<sup>20–22</sup> from the Hellmann-Feynman theorem. The electronic-structure calculations reported here are implemented on a real-space multigrid<sup>23–25</sup> using a high-order finite difference method.<sup>26,27</sup> We have used the generalized gradient approximation by Perdew *et al.*<sup>28</sup> for the exchange-correlation functional and the norm-conserving pseudopotential by Troullier and Martins.<sup>29,30</sup>

We have implemented the real-space DFT algorithm on parallel computers using spatial decomposition,<sup>31,32</sup> in which grid points are divided into spatial subregions and distributed among processors. Simulations have been carried out on 64 dual-processor nodes of an Intel Xeon/Pentium 4 based LINUX cluster.

The simulated system consists of a RDX molecule

( $C_3N_6O_6H_6$ , see Fig. 1) on a slab of 64 aluminum atoms representing four layers of Al(111) surface. The initial configuration of the RDX molecule is taken from neutron-diffraction data.<sup>33</sup> The structures of the RDX and Al(111) are optimized individually before starting the simulations. The RDX molecule is placed so that each oxygen atom is at  $\sim 2$  Å and not less than this distances from the nearest aluminum atom.

Three different initial configurations are shown as top and side views in Fig. 2. Here the  $z$  axis is parallel to the Al(111) direction. In configuration (a), the RDX molecule is placed so that its center, which is determined as the center of the three midpoints of O1–O2, O3–O4, and O5–O6, is directly above an aluminum atom in the top layer. In the configuration shown in Fig. 2(b), the RDX molecule is rotated by  $60^\circ$  in the  $x$ - $y$  plane from configuration (a). In configuration (c), the RDX molecule is translated in the  $x$ - $y$  plane from configuration (a) so that the center of the molecule is placed directly above an aluminum atom in the second layer. The periodic boundary condition is applied in all directions. A vacuum layer of thickness of 7.67 Å is inserted in the  $z$  direction to eliminate spurious interaction between periodic images. The initial temperature of the system is 0 K. The time step for the MD simulation is 0.4837 fs, and the total simulation time for each configuration is 967.4 fs (2000 steps).

### III. SIMULATION RESULTS

Figure 3 shows snapshots of the simulation with configuration (a) in Fig. 2 as the initial setup [called simulation (a) in the following]. In this figure, two atoms are connected by bonds if they are closer than the following distances: 1.4 Å for C–H bond, 1.75 Å for C–N, 1.7 Å for N–N, 1.5 Å

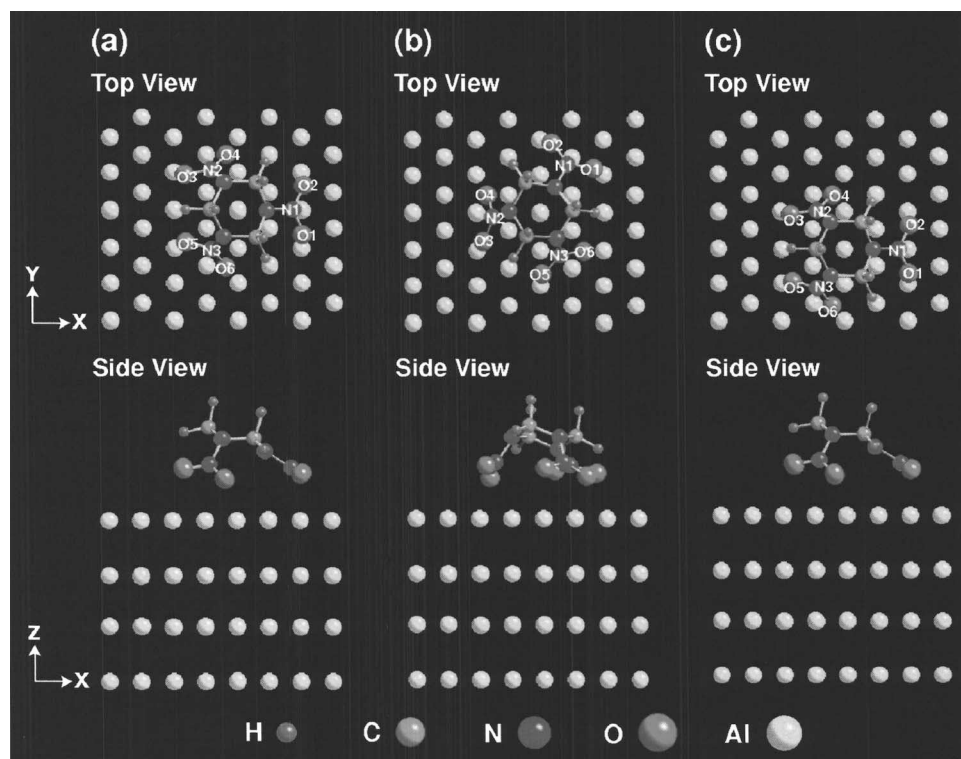


FIG. 2. Initial configurations of the RDX/Al(111) system for simulations (a), (b), and (c). A slab of 64 aluminum atoms (yellow color) represents four layers of Al(111) surface. In configuration (a), the RDX molecule is placed so that its center is directly above an aluminum atom in the top layer. In configuration (b), the RDX molecule is rotated by  $60^\circ$  in the  $x$ - $y$  plane. In configuration (c), the RDX molecule is translated in the  $x$ - $y$  plane from configuration (a) so that its center is directly above an aluminum atom in the second layer. Color represents atomic species: cyan for H, magenta for C, green for N, red for O, and yellow for Al.

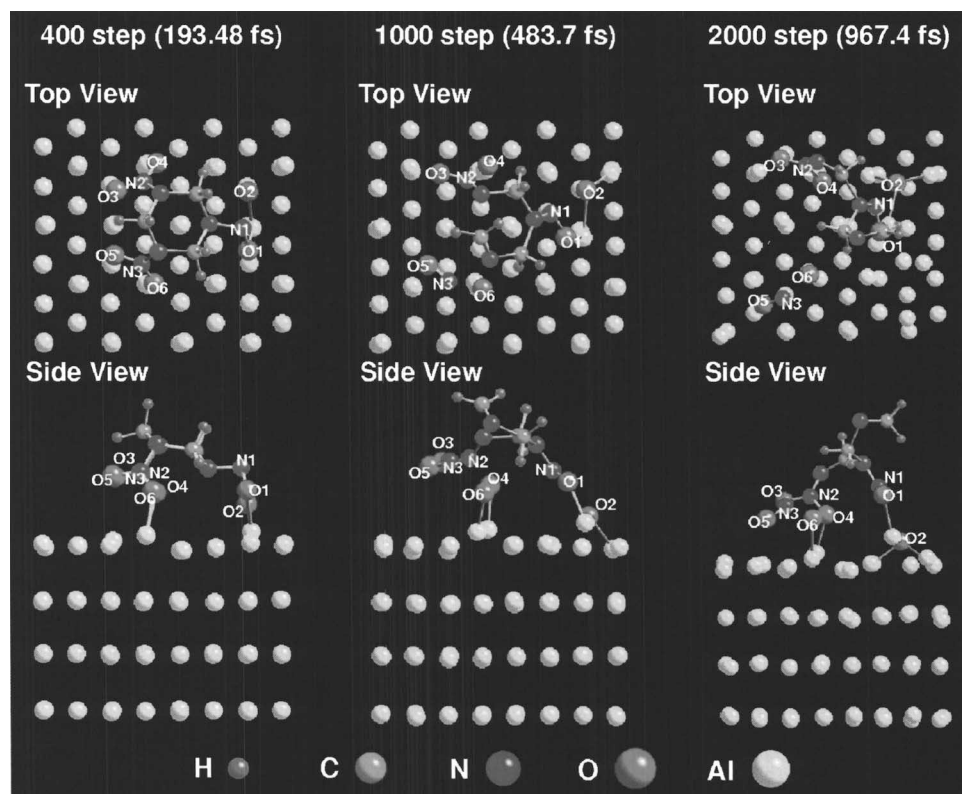


FIG. 3. Snapshots in simulation (a) with the initial configuration shown in Fig. 2(a). At the beginning of the simulation (193.48 fs), N1–O2 bond is broken and O2 starts bonding with an aluminum atom. Some other oxygen atoms are also bonding with aluminum atoms. Subsequently, more N–O bonds (N2–O4 and N3–O6) and a N–N are broken (483.7 fs), resulting in producing a NO fragment (denoted as N3–O5). Moreover, a ring of RDX, which consists of three carbon and three nitrogen atoms, is opened by a C–N bond breaking. In the end of the simulation (967.4 fs), several oxygen atoms are completely dissociated from the RDX molecule and they oxidize the Al surface. The rest of the molecule is, however, still attached to the surface.

for N–O, and 2.1 Å for Al–O. These cutoff distances are determined by the averaged bond length of each pair in the RDX molecule and Al–O bond length in alumina, plus 0.3 Å to accommodate thermal fluctuations.

At the beginning of the simulation (193.48 fs), a relatively strong N–O bond (denoted as N1 and O2) in the RDX molecule is broken. Moreover, C–N bond distances are increased about 5% on average compared to those in a RDX single molecule. Subsequently, more N–O bonds and a N–N bond are broken (483.7 fs), resulting in well-known decomposition products of RDX, i.e., NO fragments. Although the N–N bond breakage is known as the most plausible initial decomposition of the gas-phase RDX, N–O bonds are initially broken instead in our simulation of RDX on Al(111). This may be due to the strong attractive interaction between O and Al atoms. Moreover, a ring cleavage of RDX, where a ring composed of three carbon and three nitrogen atoms is opened by a C–N bond breaking, is observed at this stage. However, the ring cleavage in our simulation is slightly different from the ring fission known as an initial decomposition pathway of the gas-phase RDX in which three C–N bonds are simultaneously broken to form three  $\text{CH}_2\text{NNO}_2$ .<sup>34–36</sup> The difference may be attributed to the presence of Al(111), which changes the strength of C–N bonds. At the end of the simulation (967.4 fs), several oxygen atoms are completely dissociated from the RDX molecule and they oxidize the Al surface. The O–N fragment (denoted as O5–N3 in Fig. 3), which was dissociated from the RDX molecule at about 1000 steps, is approaching to the Al(111) surface. The distance between O5 and the nearest Al atom is reduced from 3.6 Å at 1000 steps to 2.6 Å at 2000 steps, indicating that the O–N fragment is physically adsorbed to the surface. The rest of the molecule is also attached to the

surface. We did not observe another decomposition pathway of RDX, i.e., HONO elimination<sup>16</sup> in our simulations.

In Fig. 4, the snapshots at 967.4 fs are compared with those of the other two simulations with the initial configurations (b) and (c) in Fig. 2 [called simulation (b) and (c) in the following]. Overall characteristics are the same as in simulation (a): N–O and N–N bond breaking, ring cleavage, and surface oxidation. The only difference is that more oxygen atoms oxidize aluminum surface in simulation (b) and (c) than in simulation (a). From the detailed analysis of these simulation results, we found that the RDX ring cleavage is preceded by a N–N bond breaking near a C–N bond. This suggests that the N–N bond breakage significantly weakens the C–N bonds, of which the ring consists.

In all the simulations presented in this paper, RDX molecules are initially oriented in such a way that the plane defined by the three midpoints of two oxygen atoms is parallel to the Al(111) surface. Though detailed decomposition pathways may differ for different initial orientations of the RDX molecule, the main conclusion that the initial decomposition is O–N bond breakage is likely to remain most plausible due to the strong chemical reaction between Al and O atoms. In our simulations, we have not observed any Al–N bond formation, although aluminum nitride is a well-known product of nanoaluminum exposed in nitrogen containing environment. This again may be due to the initial configuration, in which oxygen atoms in RDX are placed much closer to the Al(111) surface than nitrogen atoms are. We are currently investigating possible Al–N bond formation in different configurations, in which nitrogen atoms in RDX are placed closer to Al(111).

Figure 5 shows the total and potential energies as a function of time in simulation (a). The total energy is well con-

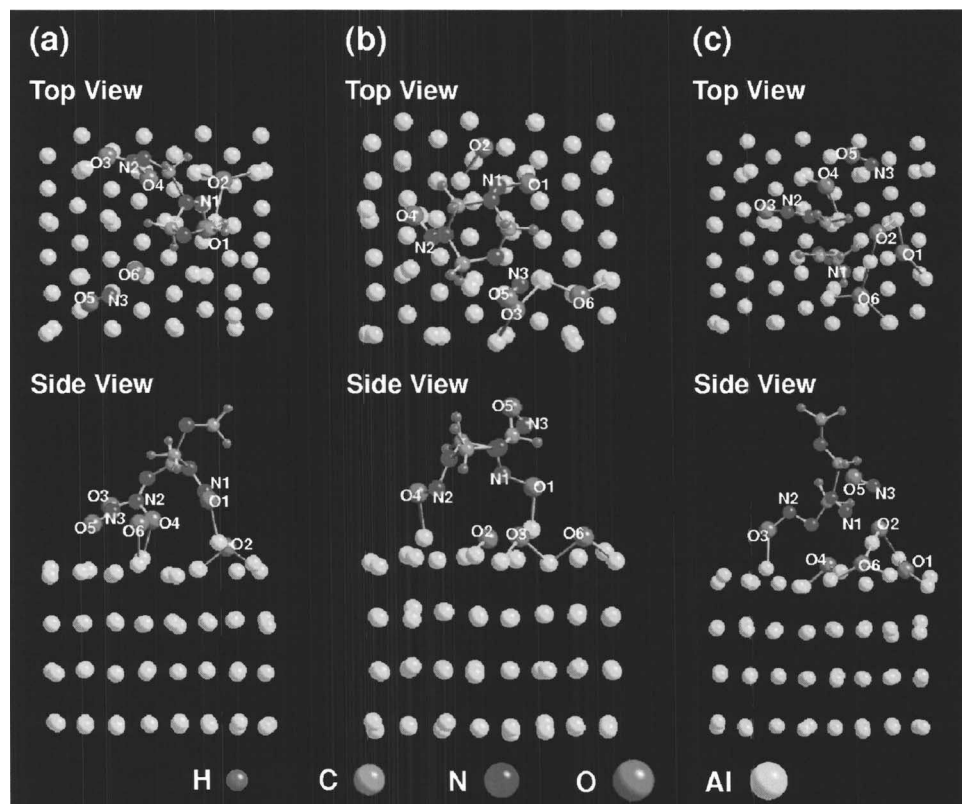


FIG. 4. Comparison of the snapshots at 2000 steps (967.4 fs) in simulation (a), (b), and (c) which are, respectively, given by the initial configurations (a), (b), and (c) shown in Fig. 2. In simulation (b) and (c), more oxygen atoms oxidize aluminum surface than in simulation (a). The rest of the molecules are still attached to the Al surface in all cases.

served during the entire simulation. The initial decrease in the potential energy indicates that there is no potential barrier for the reaction. From the decrease of the potential energy, one can roughly estimate the binding energy ( $\sim 5$  eV) between a RDX molecule and an Al(111) surface in the final configuration, corresponding to 2000 steps in Fig. 3.

In Fig. 6, the temperatures of atomic species are compared with those of RDX and the total system in simulation (a). The increase in temperature of the system indicates the occurrence of exothermic chemical reactions. The temperature of oxygen atoms is especially high because of their reactions with the aluminum surface. There are large fluctuations in temperatures corresponding to carbon and nitrogen atoms. These strong thermal fluctuations cause the ring cleavage of the RDX molecule. On the other hand, the

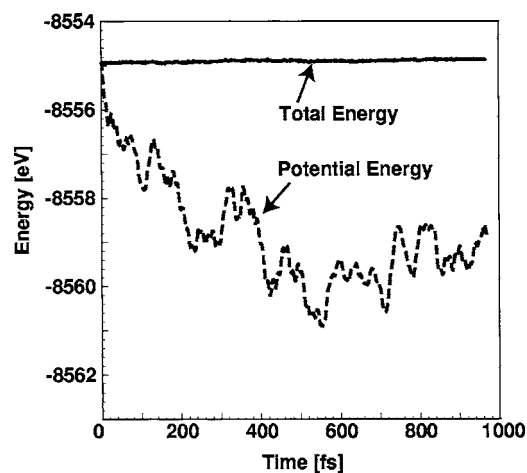


FIG. 5. Total and potential energies as a function of time in simulation (a).

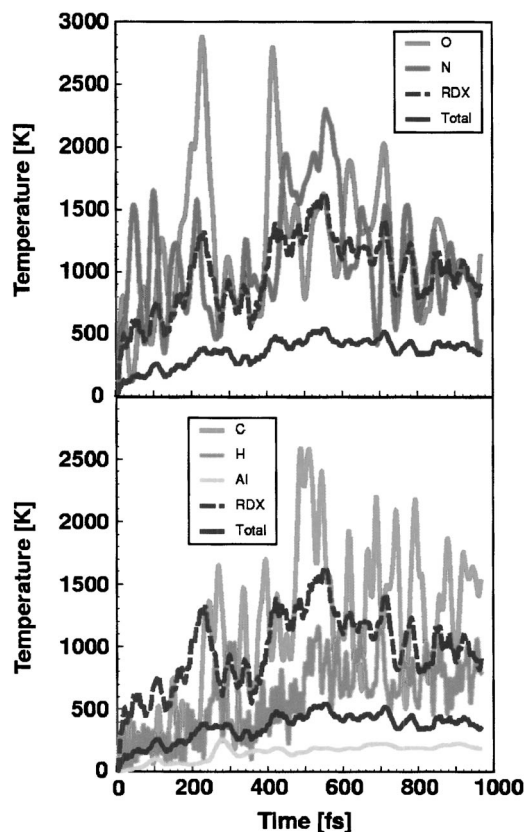


FIG. 6. Temperatures of O and N atoms (upper panel), and C, H, and Al atoms (lower panel), in comparison with that of the RDX molecule and the total system for simulation (a).

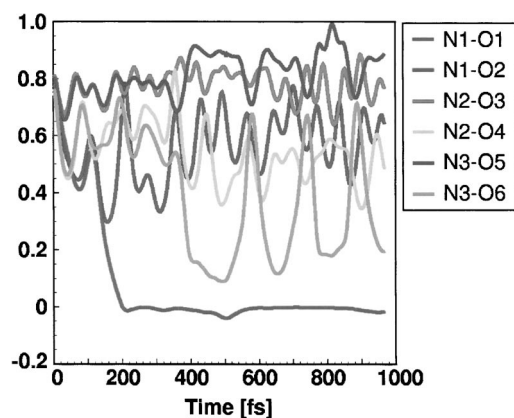


FIG. 7. Time variation of the Mulliken overlap populations of N–O bonds in simulation (a). N1–O2 bond is weakened and completely broken after 200 fs. The overlap populations of N1–O1, N2–O4, and N3–O6 bonds are decreased from the initial value of 0.8.

temperature of hydrogen is relatively low and fluctuates less than those of the other species. This is probably the reason why we do not observe the HONO elimination from RDX, for which bond formation between a hydrogen atom and an oxygen atom is required. Since hydrogen atoms are initially bonded with carbon atoms, strong thermal fluctuations are needed to break the C–H bond and to form an O–H bond. The temperature ( $\sim 200$  K) of aluminum atoms in our simulations is relatively low compared to typical combustion conditions of Al particles. We are currently studying the stability of RDX fragments on Al(111) surface at higher temperatures.

To quantitatively analyze bond breakage, we use Mulliken overlap populations.<sup>37,38</sup> The projected Kohn-Sham orbital  $\phi_i(\mathbf{r})$  onto a subspace generated by the atomic pseudo-wave-functions  $u_{rk}(\mathbf{r})$  is expressed as<sup>39</sup>

$$\phi_i(\mathbf{r}) = \sum_{rk} c_{irk} u_{rk}(\mathbf{r}), \quad (1)$$

where  $r$  and  $k$  denote atomic orbitals and atoms, respectively. The overlap population  $n(k, l)$  between the  $k$ th and  $l$ th atoms is calculated<sup>39</sup> from the coefficients  $c_{irk}$  and the overlap integral defined as

$$S_{rksl} = \int u_{rk}(\mathbf{r}) u_{sl}(\mathbf{r}) d\mathbf{r}. \quad (2)$$

A large value of  $n(k, l)$  indicates that the bond between the  $k$ th and  $l$ th atoms is strong.

Figure 7 shows the Mulliken overlap populations of N–O bonds in simulation (a). From Fig. 7, it is evident that N1–O2 bond is weakened and completely broken after 200 fs [the numbering of atoms is defined in Fig. 2(a)]. The strengths of the other N–O bonds oscillate with time. Moreover, the overlap populations for N1–O1, N2–O4, and N3–O6 bonds are less than the initial value of 0.8. These bonds may be weakened by the presence of the aluminum surface. We will confirm this conjecture in the following discussions.

In Fig. 8, we show the overlap population between each oxygen atom and all 64 aluminum atoms,

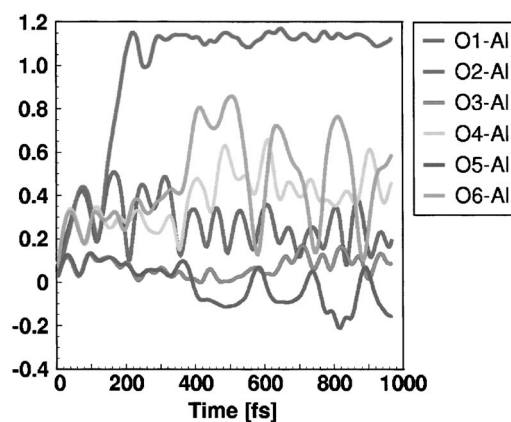


FIG. 8. Time variation of the Mulliken overlap populations of O–Al bonds in simulation (a). N1–O2 bond breaking shown in Fig. 7 results in consisting of O2–Al bonds after 200 fs. Correlated with the reduction of N1–O1, N2–O4, and N3–O6 pair overlap populations in Fig. 7, O1–Al, O4–Al, and O6–Al populations are enhanced.

$$n_{O_k-Al} = \sum_{l=1}^{64} n(O_k, Al_l), \quad (3)$$

in simulation (a). Here,  $O_k$  and  $Al_l$  denote the  $k$ th oxygen and  $l$ th aluminum atoms, respectively. Figure 8 shows that the overlap population of O2–Al is increased in time, and we consider the O2 atom to be bonded with some aluminum atoms after 200 fs. (This is consistent with Fig. 3, in which the O2 atom is bonded to one of the Al atoms.) The O2 atom is completely dissociated from the RDX molecule because of the breakage of the N1–O2 bond after 200 fs (see Fig. 7), and it oxidizes the aluminum surface. Correlated with the reduction of N1–O1, N2–O4, and N3–O6 pair overlap populations in Fig. 7, O1–Al, O4–Al, and O6–Al populations are enhanced. This analysis quantitatively confirms the conjecture that the weakening of N–O bonds is attributed to the formation of O–Al bonds.

Figures 9 and 10 show the Mulliken overlap populations for N–O and O–Al bonds in simulation (b). A major differ-

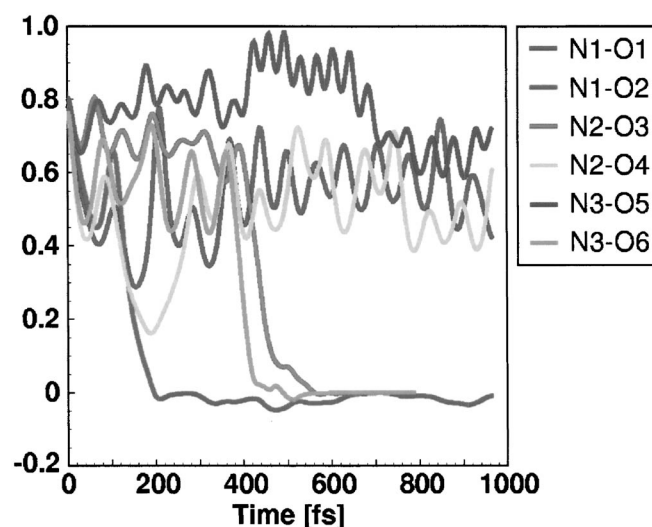


FIG. 9. Time variation of the Mulliken overlap populations of N–O bonds in simulation (b). Three N–O bonds (N1–O2, N2–O3, and N3–O6) are completely broken.

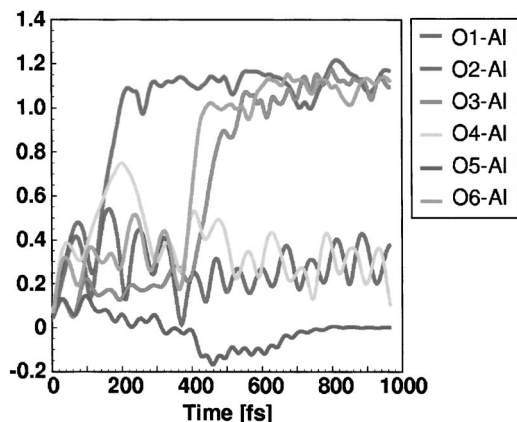


FIG. 10. Time variation of the Mulliken overlap populations of O–Al bonds in simulation (b). Correlated with the N1–O2, N2–O3, and N3–O6 bond breaking, the overlap populations of O2–Al, O3–Al, and O6–Al are enhanced.

ence from simulation (a) is that three oxygen atoms are dissociated from RDX due to the breakage of N–O bonds and are adsorbed on the aluminum surface, forming O–Al bonds. This shows that the degree of oxidization is sensitive to the position of RDX on the Al surface.

In order to study charge transfer among atoms, we calculated atomic charges as follows. The charge on the  $k$ th atom  $Q(k)$  is given by the Mulliken atomic population  $N(k)$ ,<sup>39</sup>

$$Q(k) = N_0(k) - N(k), \quad (4)$$

where  $N_0(k)$  is the number of electrons in the ground state of the free neutral atom  $k$ .

In Fig. 11, the charge distribution of each oxygen atom is shown for simulation (b). Since O2, O3, and O6 atoms are bonded with aluminum atoms as shown in Fig. 10, these oxygen atoms attract more electrons from the surrounding aluminum atoms. As a result, the absolute value of charges on oxygen atoms suddenly increases after the onset of O–Al bond formations, i.e., 100 fs for O2, 400 fs for O3, and 360 fs for O6 (see Fig. 10). On the other hand, aluminum

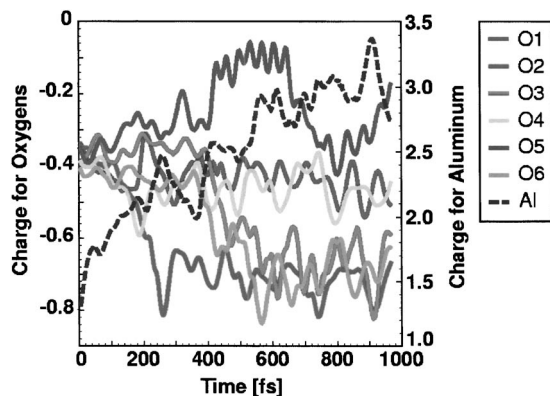


FIG. 11. Time variation of charge distribution on each oxygen atom and sum of charges of all 64 aluminum atoms in simulation (b). As a result of O2–Al, O3–Al, and O6–Al bond formation shown in Fig. 10, absolute values of charges for O2, O3, and O6 are increased by electron transfer from aluminum atoms to these oxygen atoms. On the other hand, aluminum atoms are positively charged because of the oxidization.

atoms are positively charged because of the oxidization. Figure 11 also shows the sum of charges for all 64 aluminum atoms in simulation (b). The increase of Al charges reflects the electron transfer from aluminum atoms to oxygen atoms. These electron-transfer processes cause N–O bond breakage and Al–O bond formation.

#### IV. CONCLUSIONS

We have performed first-principles molecular dynamics simulations to study the chemical reaction of a 1,3,5-trinitro-1,3,5-triazine (RDX) molecule on Al(111) surface. The RDX molecule has been found to decompose through the breakage of N–O and N–N bonds due to the strong attractive interaction between oxygen and aluminum atoms. Consequently, Al(111) surface is readily oxidized without potential barrier. The rest of the RDX molecule is adsorbed on the Al(111) surface, which prohibits further oxidation of Al in air, although the stability of the RDX fragments on Al(111) at higher temperatures remains to be studied in the future. This suggests the possibility of using RDX as a coating material for aluminum particles.

#### ACKNOWLEDGMENTS

This work was partially supported by AFOSR-DURINT, ARO-MURI, DARPA-PROM, DOE, and NSF. Parallel simulations were performed on the HPC cluster at the Research Computing Facility and the Linux clusters at the Collaboratory for Advanced Computing and Simulations at the University of Southern California.

- <sup>1</sup>P. Bucher, R. A. Yetter, F. L. Dryer, E. P. Vicenzi, T. P. Parr, and D. M. Hanson-Parr, *Combust. Flame* **117**, 351 (1999).
- <sup>2</sup>D. W. Brenner, D. H. Robertson, M. L. Elert, and C. T. White, *Phys. Rev. Lett.* **76**, 2202 (1996).
- <sup>3</sup>R. A. Yetter, F. L. Dryer, M. T. Allen, and J. L. Gatto, *J. Propul. Power* **11**, 683 (1995).
- <sup>4</sup>N. E. Schultz, G. Staszewska, P. Staszewski, and D. G. Truhlar, *J. Phys. Chem. B* **108**, 4850 (2004).
- <sup>5</sup>N. E. Schultz and D. G. Truhlar, *J. Chem. Theory Comput.* **1**, 41 (2005).
- <sup>6</sup>E. L. Dreizin, *Combust. Flame* **105**, 541 (1996).
- <sup>7</sup>P. Politzer, P. Lane, and M. E. Grice, *J. Phys. Chem. A* **105**, 7473 (2001).
- <sup>8</sup>Y. S. Kwon, A. A. Gromov, A. P. Ilyin, E. M. Popenko, and G. H. Rim, *Combust. Flame* **133**, 385 (2003).
- <sup>9</sup>T. J. Campbell, R. K. Kalia, A. Nakano, P. Vashishta, S. Ogata, and S. Rogers, *Phys. Rev. Lett.* **82**, 4866 (1999).
- <sup>10</sup>T. J. Campbell, G. Aral, S. Ogata, R. K. Kalia, A. Nakano, and P. Vashishta, *Phys. Rev. B* **71**, 205413 (2005).
- <sup>11</sup>Y. Q. Yang, Z. Y. Sun, S. F. Wang, and D. D. Dlott, *J. Phys. Chem. B* **107**, 4485 (2003).
- <sup>12</sup>Y. Q. Yang, S. F. Wang, Z. Y. Sun, and D. D. Dlott, *Appl. Phys. Lett.* **85**, 1493 (2004).
- <sup>13</sup>R. J. Jouet, A. D. Warren, D. M. Rosenberg, V. J. Bellitto, K. Park, and M. R. Zachariah, *Chem. Mater.* **17**, 2987 (2005).
- <sup>14</sup>W. H. Wilson (private communication).
- <sup>15</sup>R. A. Fifer, in *Fundamentals of Solid-Propellant Combustion*, edited by K. K. Kuo and M. Summerfield (AIAA, New York, 1984), Vol. 90, p. 177.
- <sup>16</sup>D. Chakraborty, R. P. Muller, S. Dasgupta, and W. A. Goddard, *J. Phys. Chem. A* **104**, 2261 (2000).
- <sup>17</sup>E. W. Price, in *Fundamentals of Solid-Propellant Combustion*, edited by K. K. Kuo and M. Summerfield (AIAA, New York, 1984), Vol. 90, p. 479.
- <sup>18</sup>Z. Ji and L. Shufen, *Propellants, Explos., Pyrotech.* **24**, 224 (1999).
- <sup>19</sup>A. Strachan, A. C. T. van Duin, D. Chakraborty, S. Dasgupta, and W. A. Goddard, *Phys. Rev. Lett.* **91**, 098301 (2003).

- <sup>20</sup> P. Hohenberg and W. Kohn, Phys. Rev. **136**, B864 (1964).
- <sup>21</sup> W. Kohn and L. J. Sham, Phys. Rev. **140**, A1133 (1965).
- <sup>22</sup> W. Kohn and P. Vashishta, in *Inhomogeneous Electron Gas*, edited by N. H. March and S. Lundqvist (Plenum, New York, 1983), p. 79.
- <sup>23</sup> J. L. Fattebert and J. Bernholc, Phys. Rev. B **62**, 1713 (2000).
- <sup>24</sup> T. L. Beck, Rev. Mod. Phys. **72**, 1041 (2000).
- <sup>25</sup> S. Ogata, F. Shimojo, R. K. Kalia, A. Nakano, and P. Vashishta, Comput. Phys. Commun. **149**, 30 (2002).
- <sup>26</sup> J. R. Chelikowsky, N. Troullier, K. Wu, and Y. Saad, Phys. Rev. B **50**, 11355 (1994).
- <sup>27</sup> J. R. Chelikowsky, N. Troullier, and Y. Saad, Phys. Rev. Lett. **72**, 1240 (1994).
- <sup>28</sup> J. P. Perdew, K. Burke, and M. Ernzerhof, Phys. Rev. Lett. **77**, 3865 (1996).
- <sup>29</sup> N. Troullier and J. L. Martins, Phys. Rev. B **43**, 1993 (1991).
- <sup>30</sup> N. Troullier and J. L. Martins, Phys. Rev. B **43**, 8861 (1991).
- <sup>31</sup> F. Shimojo, R. K. Kalia, A. Nakano, and P. Vashishta, Comput. Phys. Commun. **140**, 303 (2001).
- <sup>32</sup> F. Shimojo, R. K. Kalia, A. Nakano, and P. Vashishta, Comput. Phys. Commun. **167**, 151 (2005).
- <sup>33</sup> C. S. Choi and E. Prince, Acta Crystallogr., Sect. B: Struct. Crystallogr. Cryst. Chem. **28**, 2857 (1972).
- <sup>34</sup> X. Zhao, E. J. Hints, and Y. T. Lee, J. Chem. Phys. **88**, 801 (1988).
- <sup>35</sup> D. Habibollahzadeh, M. Grodzicki, J. M. Seminario, and P. Politzer, J. Phys. Chem. **95**, 7699 (1991).
- <sup>36</sup> C. J. Wu and L. E. Fried, J. Phys. Chem. A **101**, 8675 (1997).
- <sup>37</sup> R. S. Mulliken, J. Chem. Phys. **23**, 1833 (1955).
- <sup>38</sup> R. S. Mulliken, J. Chem. Phys. **23**, 1841 (1955).
- <sup>39</sup> D. Sanchez-Portal, E. Artacho, and J. M. Soler, J. Phys.: Condens. Matter **8**, 3859 (1996).